Neuroligin-1–dependent competition regulates cortical synaptogenesis and synapse number

Hyung-Bae Kwon[1,3], Yevgenia Kozorovitskiy[1], Won-Jong Oh[2], Rui T Peixoto[1], Nazia Akhtar[1], Jessica L Saulnier[1], Chenghua Gu[2] & Bernardo L Sabatini[1]

Members of the neuroligin family of cell-adhesion proteins are found at excitatory and inhibitory synapses and are mutated in some familial forms of autism spectrum disorders. Although they display synaptogenic properties in heterologous systems, the function of neuroligins *in vivo* in the regulation of synapse formation and synapse number has been difficult to establish. We found that neuroligin-1 (NL1), which is located at excitatory postsynaptic densities, regulates activity-dependent synaptogenesis and mature synapse number on cortical layer 2/3 pyramidal neurons *in vivo*. However, synapse number was not sensitive to absolute NL1 levels but instead depended on transcellular differences in the relative amounts of NL1. These effects were independent of the cell-autonomous regulation of NMDA-type glutamate receptors by absolute levels of NL1. Our data indicate that transcellular competitive processes govern synapse formation and number in developing cortex and that NL1 has a central function in these processes.

Neocortical development progresses through stages of synaptogenesis and synapse refinement that establish cell-to-cell connectivity and network topology[1,2]. During early development, intrinsically generated patterned activity helps establish the correct connectivity between and in brain regions[3,4]. During later development, perturbations of sensory experience of the animal alter connectivity in sensory cortices, indicating that the activity-dependent control of synaptogenesis shapes postnatal development[5–7]. In addition, molecular cues, including gradients of signaling molecules and intercellular cell-adhesion complexes, regulate many aspects of circuit and cellular development[8–11]. Thus, postnatal development of cerebral cortex is governed by activity-dependent and activity-independent mechanisms that regulate synaptic connectivity.

Trans-synaptic cell-adhesion molecules, which are present at synapses and mediate transcellular and intracellular signals, regulate both activity-dependent and activity-independent synaptic maturation during development[9,10,12,13]. The neuroligin family of proteins, which consists of synaptically localized cell-adhesion molecules that are expressed in a developmentally regulated manner, has been proposed to regulate many aspects of synaptic transmission and development[14,15]. Four neuroligins have been identified in mice, and localization of each family member varies[16–18]. For example, NL1 is predominantly postsynaptic at excitatory synapses[14] and binds to presynaptic neurexins, an interaction that is thought to act after initial synapse formation to regulate synapse maturation[19]. In contrast, NL2 is found predominantly at inhibitory synaptic terminals[15] and regulates assembly of GABAergic synapses[20]. The importance of neuroligin-dependent signaling to human brain development is highlighted by the finding of mutations in neuroligins and neurexins in families with genetic forms of autism[21–23].

Defining the functions of NL1 in synapse development and separating its transcellular versus cell-autonomous contributions has been difficult. Up- and downregulation of NL1 increases and decreases, respectively, synaptic currents mediated by NMDA-type glutamate receptors (NMDARs)[19,24–26] (but see ref. 15). However, whether the number and structure of excitatory synapses are regulated by NL1 remains unclear, and results from studies of various preparations are in conflict. NL1 expressed in non-neuronal cells attracts axons and induces formation of rudimentary presynaptic boutons[27], suggesting that NL1 is intrinsically synaptogenic. In cultured neurons, the number of glutamatergic synapses increases with overexpression of NL1 (refs. 19,28–34) and decreases with knockdown of NL1 with RNA interference (RNAi)[29]. On the other hand, despite a perinatal lethal phenotype and perturbations of synaptic transmission in respiratory nuclei, neurons from NL1, NL2 and NL3 triple knockout mice have a normal number of synapses and normal synaptic ultrastructure[15]. Similarly, loss of NL1 in hippocampus or amygdala has been reported to not alter synapse number[15,24,25]. Thus, studies of cultured neurons whose NL1 levels have been manipulated *ex vivo* indicate that NL1 regulates synapse number and spine morphology, whereas analyses *in vivo* or of tissue acutely prepared from knockout animals have not supported this conclusion.

A possible explanation for these conflicting results is that differences in activity patterns between neurons in culture and *in vivo* may reveal or mask the effects of NL1 manipulation, a hypothesis that is consistent with the dependence of the synaptic effects of NL1 overexpression on activity levels in cultured neurons[19]. Alternatively,

differences may arise as a result of the timing of the manipulation, the brain region examined or the fraction of neurons that are affected.

To determine whether NL1 regulates the formation, morphology and function of excitatory synapses *in vivo*, we examined cortical layer 2/3 pyramidal neurons whose levels of NL1 had been up- or downregulated from the time of neuronal birth. Synapse structure and function in tissue in which all neurons lacked NL1 was compared with that in genetically mosaic tissue in which NL1 levels varied from cell to cell. Analysis in acute brain slices revealed that early postnatal defects in NMDARs were triggered by both global and sparse loss of NL1. Conversely, NL1-dependent changes in synapse number and activity-dependent synaptogenesis were revealed only when differences in NL1 levels existed across neurons. For this reason, the effects of NL1 knockdown or overexpression were different in wild-type, NL1 heterozygote and NL1 null mice. Thus, transcellular differences in NL1 levels during development, but not the absolute levels of NL1 in individual cells, regulate activity-dependent synaptogenesis and determine the mature structure and function of cortical neurons.

RESULTS

Modulation of synapse number by sparse knockdown of NL1

To determine whether postsynaptic NL1 levels regulate synapse development *in vivo*, we induced RNAi to knockdown NL1 in cortical neurons using *in utero* electroporation. Electroporation at embryonic stage 15.5, when progenitors for layer 2/3 cortical neurons are accessible, resulted in sparse transfection (up to ~20%) of layer 2/3 pyramidal neurons while allowing neurons to develop *in vivo* under largely normal network activity and connectivity (**Fig. 1a**).

Plasmids encoding small-hairpin RNAs (shRNA) with sequence homology to mouse *Nlgn1* were designed and purchased (Online Methods). Constructs were tested *in vitro* for knockdown of an NL1-EGFP fusion protein in HEK293 cells (**Fig. 1b** and **Supplementary Fig. 1**). The most effective construct, sh-NL1 #7, was used for the majority of subsequent experiments and we refer to it as sh-NL1. This construct was effective in neurons, as transduction of dissociated cortical cultures with lentiviruses encoding the plasmid strongly reduced endogenous NL1 levels (**Fig. 1c** and **Supplementary Fig. 1**). Reduction of NL1 expression did not substantially alter levels of the family members NL2 and NL3 (**Fig. 1d** and **Supplementary Fig. 1**).

Examination of dendritic spines of sh-NL1 expressing neurons in acute slices prepared from postnatal day 17–21 *in utero* electroporated mice revealed that spine length and head area were increased and spine density was reduced compared with control EGFP-transfected neurons (sh-NL1, 0.50 ± 0.06 spines per μm; control, 0.91 ± 0.04 spines per μm; 11–17 neurons, 25–27 dendrites, $P < 0.05$; **Fig. 1e** and **Supplementary Fig. 2a**). Co-transfection of sh-NL1 and *NLGN1* (human NL1), which contains sequence alterations in the region targeted by sh-NL1, suppressed the effects of NL1 knockdown (0.93 ± 0.05 spines per μm, 10 neurons, 22 dendrites, $P > 0.05$ versus control; **Fig. 1e** and **Supplementary Fig. 2a**), indicating that spine changes in sh-NL1–expressing neurons were the result of loss of NL1. Similar morphological changes were observed in biolistically transfected hippocampal CA1 pyramidal neurons in organotypic slice cultures (**Supplementary Fig. 3**).
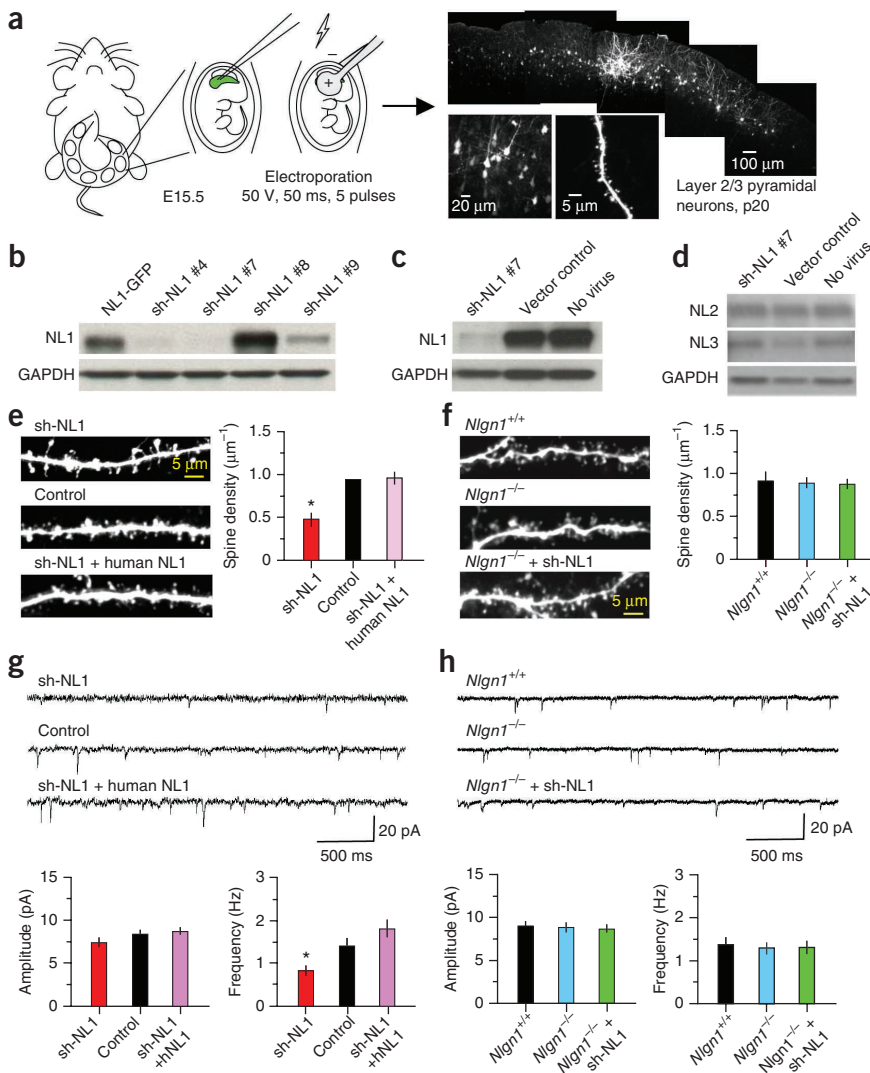

Figure 1 Sparse knockdown of NL1, but not global knockout, reduces synapse number and spine density in cortical layer 2/3 pyramidal neurons. (**a**) Left, schematic of the *in utero* electroporation method used to transfect neocortical layer 2/3 pyramidal neurons *in vivo*. Right, low- and high-magnification images of an acute slice showing EGFP expression in layer 2/3 pyramidal neurons. (**b**) Western blot analysis of knockdown efficiency in sh-NL1– and NL1-GFP–transfected HEK293T cells. (**c**,**d**) Western blot analysis of endogenous NL1, NL2 and NL3 expression in dissociated cortical cultures transduced with lentivirus encoding sh-NL1 #7 or lentivirus carrying a control vector compared with that in uninfected controls. (**e**) Top, examples and summary of spine density in layer 2/3 pyramidal neurons in acute brain slices expressing EGFP (control), sh-NL1 #7 (sh-NL1), or sh-NL1 and human NL1. Bottom, representative mEPSCs and their average amplitude and frequency for neurons of each indicated genotype. (**f**) Examples and summary of spine density (top) and mEPSCs (bottom) in acute brain slices of *Nlgn1*^{+/+}, *Nlgn1*^{–/–} and *Nlgn1*^{–/–} neurons transfected with sh-NL1. *$P < 0.05$ versus control. Error bars represent s.e.m.
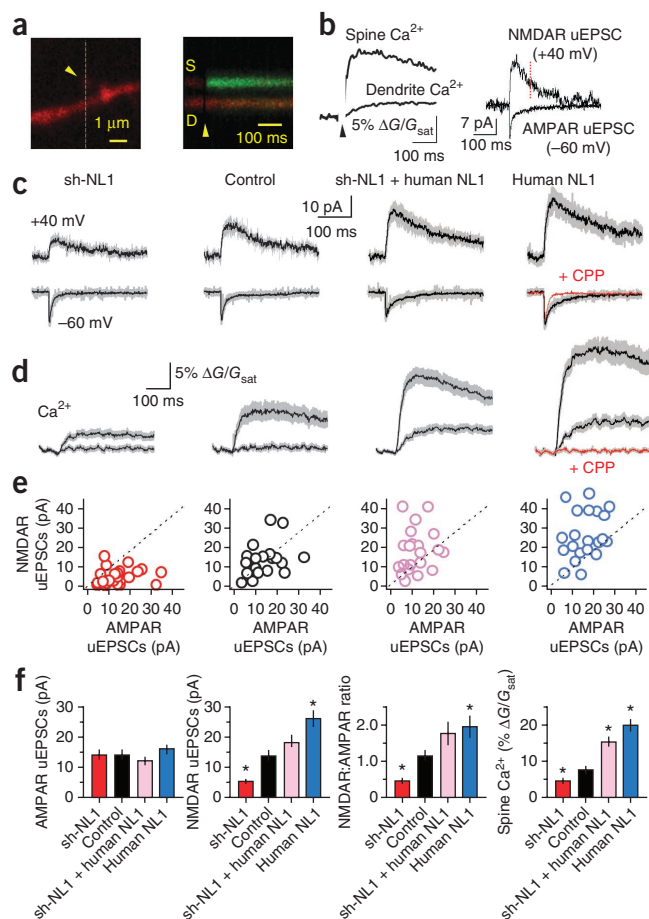
Figure 2 NL1 modulates NMDAR-mediated currents and Ca^{2+} signaling at individual postsynaptic terminals. (**a**) Left, image of a spine and dendrite filled with 20 µM Alexa-594 and 300 µM Fluo-5F showing the location of the glutamate uncaging spot (arrowhead) and the orientation of the line scan (dashed line). Right, time course of fluorescent transients measured in the line scan intersecting the spine (S) and dendrite (D) following glutamate uncaging at the time indicated by the arrowhead. Increased green fluorescence indicates Ca^{2+} entry. (**b**) Left, quantification of the green fluorescence transient in the spine and neighboring dendrite at −60 mV. Right, AMPAR- and NMDAR-mediated uEPSCs at −60 and +40 mV, respectively. The red dotted line (70 ms after uncaging pulse) indicates the time at which the amplitude of NMDAR uEPSCs was measured. (**c**) Average uEPSCs at −60 mV and +40 mV for neurons of the indicated genotypes and from *NLGN1*-transfected neurons in the presence of CPP (red trace). (**d**) Average Ca^{2+} transients in spines (larger traces) and dendrites (smaller traces) for neurons of the indicated genotypes −60 mV. (**e**) Distributions of AMPAR and NMDAR uEPSCs amplitudes for each spine in each genotype. (**f**) Summary of (left to right) AMPAR uEPSC amplitude, NMDAR uEPSC amplitude, NMDAR-to-AMPAR uEPSC amplitude ratio, and spine Ca^{2+} are shown. *$P < 0.05$ versus control. Error bars represent s.e.m.

NL1 modulates NMDAR-mediated currents and Ca^{2+} influx

A possible mechanism for NL1-dependent modulation of synapse number is by downregulation of NMDARs, which regulate synapse structure and function via a variety of mechanisms and whose activation triggers activity-dependent synaptogenesis in developing layer 2/3 pyramidal neurons[35]. To determine whether the functional properties of individual postsynaptic terminals are differentially affected by sparse versus global manipulations of NL1, we used glutamate uncaging to examine AMPA receptor (AMPAR)- and NMDAR-mediated currents and Ca^{2+} influx (**Fig. 2** and **Supplementary Fig. 4**). Whole-cell recordings were obtained from layer 2/3 pyramidal neurons using intracellular solutions containing Alexa Fluor 594 (20 µM) to visualize morphology and a Ca^{2+} indicator, Fluo-5F (300 µM), to monitor intracellular Ca^{2+}. MNI-glutamate (5 mM) in the extracellular solution was photolysed to release glutamate by two-photon excitation with 0.5-ms-long 720-nm laser pulses (**Fig. 2a**). To improve voltage clamp and monitor single terminal AMPAR and NMDAR signals, we blocked voltage-gated K^+, Na^+ and Ca^{2+} channels with a cocktail of antagonists (Online Methods). Uncaging glutamate near a visualized spine elicited uncaging-evoked AMPAR and NMDAR EPSCs (AMPAR uEPSCs and NMDAR uEPSCs) that were measured by holding cells at −60 and +40 mV, respectively (**Fig. 2b**). Simultaneous measurement of green fluorescence was used to monitor Ca^{2+} transients in the active spine and neighboring dendrite at −60 mV. Under these conditions Ca^{2+} enters the spine through NMDARs, which are not fully blocked by extracellular Mg^{2+} (refs. 36,37).

Voltage-clamp recordings from sh-NL1–transfected neurons did not reveal significant differences in AMPAR uEPSCs compared with control (sh-NL1, 14.0 ± 1.6 pA, $n = 25$; control, 14.2 ± 1.7, $n = 20$; $P > 0.05$; **Fig. 2c,f**). At these same postsynaptic terminals, however, NMDAR uEPSCs (sh-NL1, 5.0 ± 0.8 pA, $n = 25$; control, 13.7 ± 1.8 pA, $n = 20$; $P < 0.05$) and Ca^{2+} transients ($\Delta G/G_{sat}$: sh-NL1, 4.1 ± 0.6%, $n = 25$; control, 7.6 ± 1.0%, $n = 20$; $P < 0.05$) were smaller in sh-NL1–expressing neurons (**Fig. 2c–f**), consistent with reduced NMDAR content in individual spines. Both NMDAR uEPSCs and Ca^{2+} influx were restored or increased beyond control levels by coexpression of sh-NL1 and human NL1 (NMDAR uEPSCs, 18.1 ± 2.4 pA, $n = 21$, $P > 0.05$ versus control; $\Delta G/G_{sat}$, 15.3 ± 1.4%, $n = 21$, $P < 0.05$; **Fig. 2c–f**). Similarly, larger NMDAR uEPSCs and Ca^{2+} transients were measured from spines of cells expressing human NL1 alone (NMDAR uEPSCs, 26.0 ± 2.7 pA, $n = 21$, $P < 0.05$; $\Delta G/G_{sat}$, 19.9 ± 1.7%, $n = 21$, $P < 0.05$; **Fig. 2c–f**). This positive correlation between NL1

The frequency of miniature excitatory postsynaptic currents (mEPSCs) in NL1 knockdown neurons measured by whole-cell voltage-clamp was reduced without significant effect on their amplitude (amplitude: sh-NL1, 7.40 ± 0.54 pA, $n = 8$; control, 8.36 ± 0.41 pA, $n = 10$; $P > 0.05$; frequency: sh-NL1, 0.82 ± 0.12 Hz, $n = 8$; control, 1.40 ± 0.17 Hz, $n = 10$; $P < 0.05$; **Fig. 1e**). These effects were prevented by co-transfection of *NLGN1* (amplitude, 8.71 ± 0.42 pA; frequency, 1.81 ± 0.20 Hz; $n = 10$, $P > 0.05$ versus control; **Fig. 1e**), confirming the NL1 dependence of the effects on synapse number.

Nevertheless, similar effects were not observed in layer 2/3 pyramidal neurons of *Nlgn1*$^{-/-}$ mice, which had no spine morphology or density changes compared to those in wild-type animals (*Nlgn1*$^{+/+}$, 0.91 ± 0.1 spines per µm, 9 neurons, 19 dendrites; *Nlgn1*$^{-/-}$, 0.88 ± 0.05 spines per µm, 10 neurons, 22 dendrites; $P > 0.05$; **Fig. 1f** and **Supplementary Fig. 2b**). Notably, introduction of sh-NL1 into *Nlgn1*$^{-/-}$ neurons had no effect on the structure and density of spines (*Nlgn1*$^{-/-}$ + sh-NL1, 0.87 ± 0.05 spines per µm, 10 neurons, 19 dendrites, $P > 0.05$ versus *Nlgn1*$^{+/+}$; **Fig. 1e** and **Supplementary Fig. 2b**), confirming that the effects of sh-NL1 in wild-type animals were a result of the loss of NL1 and not of possible off-target effects of the shRNA. Similarly, no changes in mEPSC amplitude and frequency were observed (frequency: *Nlgn1*$^{+/+}$, 1.35 ± 0.16 Hz, $n = 8$; *Nlgn1*$^{-/-}$, 1.28 ± 0.13, $n = 9$; *Nlgn1*$^{-/-}$ + sh-NL1, 1.30 ± 0.1, $n = 8$; amplitude: *Nlgn1*$^{+/+}$, 9.0 ± 1.5 Hz, $n = 8$; *Nlgn1*$^{-/-}$, 8.8 ± 1.7, $n = 9$; *Nlgn1*$^{-/-}$ + sh-NL1, 8.7 ± 1.3, $n = 9$; **Fig. 1f**). Thus, reduction of NL1 levels in a sparse subset of cortical neurons alters synapse number, whereas global knockout of the gene has no effect. Notably, both sets of experiments were carried out in the same cell type and in the same *in vivo* context.

1669

Figure 3 Constitutive NL1 knockout lowers NMDAR uEPSCs and Ca^{2+} transients. (**a,b**) Average AMPAR and NMDAR uEPSCs (**a**) and spine and dendrite Ca^{2+} transients at −60 mV (**b**) for neurons of the indicated genotypes. (**c**) Relationship between AMPAR and NMDAR uEPSCs measured in the indicated genotypes. (**d**) Average amplitudes of AMPAR (left) and NMDAR (middle) uEPSCs and NMDAR:AMPAR current ratios (right). *$P < 0.05$ versus wild type. Error bars represent s.e.m.

levels and NMDAR-mediated synaptic signals suggests that NL1 facilitates incorporation or retention of NMDARs in the postsynaptic terminal, consistent with previous findings[31,33,38].

The average peak amplitude of uEPSCs measured at −60 mV was not modulated by NL1 levels, but the uEPSC decay was slowed in human NL1 *(NLGN1)*-transfected neurons (**Fig. 2c**). To determine whether this prolongation resulted from alterations of AMPAR properties or whether it represented an unusual contribution of NMDAR currents at resting potentials, we repeated recordings in the presence of the NMDAR antagonist CPP (10 μM). CPP application abolished the spine and dendrite Ca^{2+} signals, as well as the slow component of uEPSC, confirming that they resulted from NMDAR activation (**Fig. 2d**).

Parallel analyses were carried out in *Nlgn1*^{−/−} mice (**Fig. 3**), in which NMDAR/AMPAR current ratios have been previously reported to be reduced in hippocampal CA1 pyramidal neurons, amygdala principal neurons and striatal medium spiny neurons[19,24,39]. Consistent with these reports, we found that glutamate uncaging–evoked AMPAR uEPSCs measured from individual spines of layer 2/3 pyramidal neurons were not different between *Nlgn1*^{−/−} and *Nlgn1*^{+/+} littermate mice, whereas NMDAR uEPSCs were significantly smaller in *Nlgn1*^{−/−} mice (AMPAR uEPSCs: *Nlgn1*^{+/+}, 10.7 ± 1.3 pA, $n = 24$; *Nlgn1*^{−/−}, 8.6 ± 1.2 pA, $n = 25$; $P > 0.05$; NMDAR uEPSCs: *Nlgn1*^{+/+}, 9.9 ± 1.2 pA, $n = 24$; *Nlgn1*^{−/−}, 4.0 ± 0.8 pA, $n = 25$; $P < 0.05$; **Fig. 3a,d**). NMDAR-mediated spine Ca^{2+} influx was also reduced ($\Delta G/G_{sat}$: *Nlgn1*^{+/+}, 8.8 ± 1.1%, $n = 24$; *Nlgn1*^{−/−}, 5.2 ± 0.6 pA, $n = 25$; $P < 0.05$; **Fig. 3b**). Furthermore, introducing sh-NL1 into *Nlgn1*^{−/−} neurons had no effect on NMDAR uEPSCs and Ca^{2+} influx, indicating that,
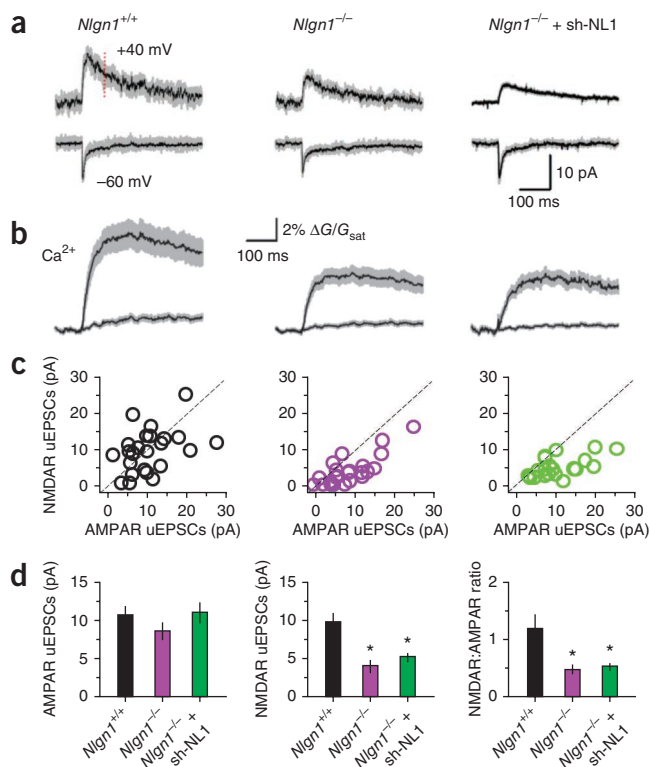
as expected for an NL1-dependent phenomenon, sh-NL1–mediated effects were occluded by constitutive loss of NL1 (*Nlgn1*^{−/−} + sh-NL1: AMPAR uEPSCs, 11.0 ± 1.3 pA; NMDAR uEPSCs, 5.2 ± 0.6 pA; $\Delta G/G_{sat}$, 4.9 ± 0.5%; $n = 20$, $P > 0.05$ for each versus *Nlgn1*^{−/−}; **Fig. 3**). Thus, the effects of NL1 loss on synaptic NMDARs are similar in the global knockout and RNAi-induced sparse knockdown, indicating that the level of NL1 in each cell intrinsically regulates NMDAR signaling but not excitatory synapse number.

NL1 levels modulate glutamate-induced spinogenesis

Overexpression of NL1 in dissociated neuronal cultures influences synapse number in an activity-dependent manner[19], suggesting that NL1 regulates the selection of synapses after initial synapse formation. To determine whether NL1 also regulates initial synapse formation, we used a glutamate uncaging protocol that triggered the rapid and *de novo* formation of a spine and the establishment of a new synapse (**Fig. 4a**)[35]. This process requires
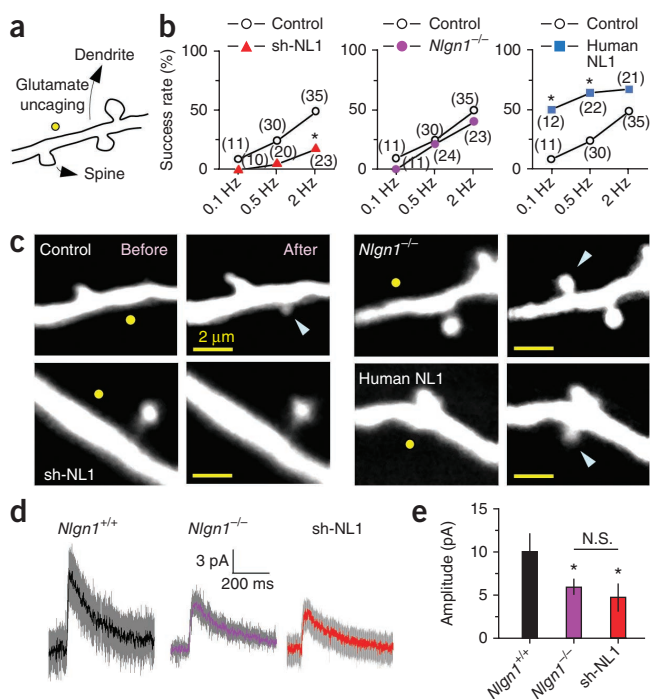

Figure 4 NL1 regulates activity-dependent spinogenesis. (**a**) Schematic of glutamate-induced spinogenesis. Dendrites of EGFP-expressing cortical layer 2/3 pyramidal neurons in acute slices from postnatal day 8–12 (P8–12) mice were visualized with two-photon laser-scanning microscopy and glutamate (40 pulses) was released by photolysis of caged glutamate near a low-spine density section of dendrite. (**b**) Success rate of *de novo* spine formation in neurons in which NL1 levels were reduced or increased. The numbers of attempts are shown in parentheses. *$P < 0.05$ versus control. (**c**) Representative images of attempted spinogenesis experiments from wild-type neurons transfected with EGFP, sh-NL1 or human NL1, and from an EGFP-transfected *Nlgn1*^{−/−} neuron. Yellow circles and blue arrowheads indicate uncaging positions and, when applicable, nascent spines, respectively. (**d,e**) Average dendritic NMDAR uEPSCs (**d**) and amplitudes (**e**) recorded at +40 mV in the presence of NBQX from P9–11 neurons of the indicated genotypes. Glutamate was released 0.5 μm from the dendritic shaft. *$P < 0.05$ versus wild type. N.S., $P > 0.05$. Error bars represent s.e.m.

Figure 5 Spine density of $Nlgn1^{-/-}$ neurons *in vitro* is affected by presence of neighboring $Nlgn1^{+/+}$ neurons. (**a**) Schematic of the co-culture experiment. $Nlgn1^{-/-}$ mice were *in utero* electroporated to label layer 2/3 pyramidal neurons with EGFP. Dissociated cortical cultures were prepared from these mice and mixed with neurons of unlabeled wild-type mice at varying ratios. (**b**) Representative low- (left) and high-magnification (right) images of neurons and spiny dendrites. Scale bars for whole-cell (left) and dendrite (right) images in **a** and **b** represent 30 μm and 10 μm, respectively. (**c**) Average spine densities in $Nlgn1^{-/-}$ neurons mixed with $Nlgn1^{+/+}$ neurons at different ratios. *$P < 0.05$ versus $Nlgn1^{-/-}$. N.S., $P > 0.05$. Error bars represent s.e.m.

activation of dendritic NMDA receptors, which are perturbed by changes in NL1 expression (see below).

In wild-type animals, sparse knockdown of NL1 in layer 2/3 pyramidal neurons by RNAi lowered, whereas overexpression of NL1 increased, the success rate of new spine generation (**Fig. 4b,c**). The magnitude of the effects depended on the frequency of stimulation such that NL1 overexpression enhanced the low probability of spinogenesis seen with low-frequency stimuli, whereas downregulation of NL1 decreased the high success rate triggered by higher frequency stimuli. In contrast, the same class of neurons in $Nlgn1^{-/-}$ mice displayed normal activity-dependent spinogenesis. Furthermore, the normal synaptogenetic potential of neurons in $Nlgn1^{-/-}$ mice occurs despite a ~50% reduction in dendritic NMDAR currents (NMDAR uEPSCs: $Nlgn1^{+/+}$, 10.0 ± 2.1 pA, $n = 15$; $Nlgn1^{-/-}$, 5.9 ± 0.9 pA, $n = 15$; $P < 0.05$; **Fig. 4d,e**), a similar reduction to that seen in sh-NL1–transfected neurons in wild-type animals (4.7 ± 0.9 pA, $n = 16$, $P > 0.05$; **Fig. 4d,e**). Thus, sparse, but not global, manipulations of NL1 modulate the threshold of activity-dependent spinogenesis, likely explaining the parallel observations in synapse and spine number at later developmental stages.

Excitatory synapse number is regulated by relative levels of NL1
The findings that synapse number and structure are altered in neurons with NL1 knockdown, but not in neurons with $Nlgn1^{-/-}$, may be explained by a transcellular competitive mechanism[40,41]. In this model, a cell expressing higher levels of NL1 relative to its neighbors has an advantage in forming synapses. For example, each
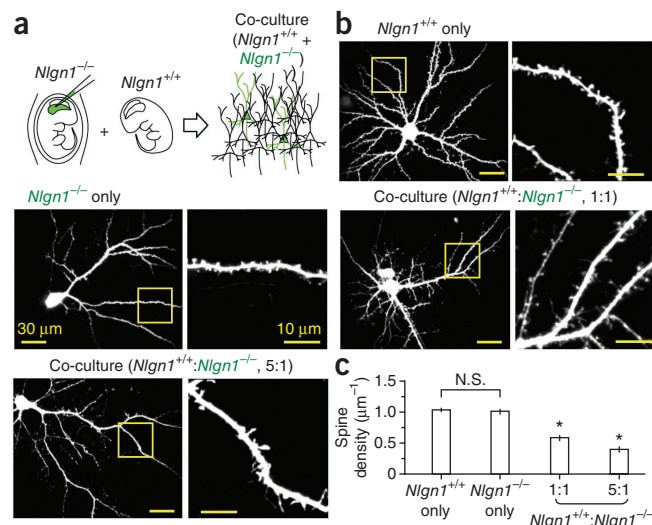
cortical neuron might compete in an NL1-dependent manner with surrounding neurons to establish proper connectivity with a limited number of presynaptic boutons. If correct, this mechanism explains why manipulations that eliminate NL1 from all neurons fail to recapitulate the perturbations seen in genetically mosaic tissue.

To test this model, we performed co-culture experiments in which $Nlgn1^{+/+}$ and $Nlgn1^{-/-}$ neurons were mixed (**Fig. 5**). We used *in utero* electroporation to transfect EGFP into layer 2/3 pyramidal neurons of $Nlgn1^{-/-}$ mice. Cultures of cortical neurons were prepared by mixing, at specific ratios, cells dissociated from these manipulated $Nlgn1^{-/-}$ mice and age-matched wild-type mice (**Fig. 5a**). Consistent with the competition hypothesis, neurons in pure cultures of $Nlgn1^{-/-}$ or $Nlgn1^{+/+}$ cells had similar spine densities ($Nlgn1^{+/+}$, 1.03 ± 0.03 spines per μm, 37 fields of view; $Nlgn1^{-/-}$, 1.01 ± 0.05 spines per μm, 21 fields of view; $P > 0.05$; **Fig. 5c**). However, when $Nlgn1^{-/-}$ cells were mixed 1:1 with $Nlgn1^{+/+}$ neurons, spine density in the $Nlgn1^{-/-}$ cells was reduced (0.58 ± 0.05 spines per μm, 16 fields of view, $P < 0.05$; **Fig. 5b,c**). Spine density was further reduced when the ratio of $Nlgn1^{-/-}$ to $Nlgn1^{+/+}$ cells was reduced to 1:5 (0.39 ± 0.04 spines per μm, 18 fields of view, $P < 0.05$; **Fig. 5c**). Thus, the spine density of $Nlgn1^{-/-}$ cortical layer 2/3 pyramidal neurons in culture depends on the fraction of co-cultured neurons that
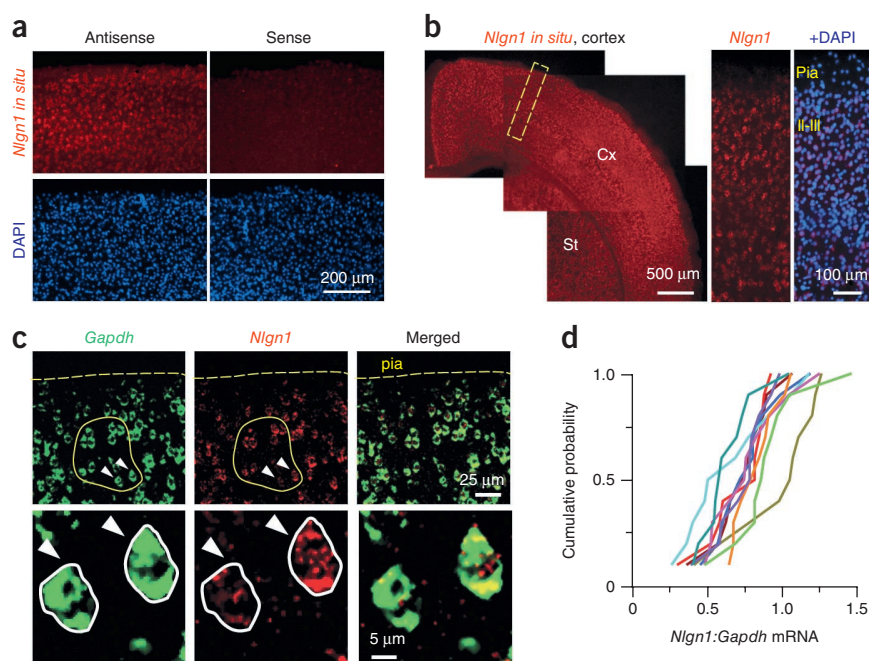

Figure 6 Variable $Nlgn1$ mRNA in across cortical neurons. (**a**) Fluorescence ISH using an antisense $Nlgn1$ riboprobe (left) revealed $Nlgn1$ mRNA detection in the cortex compared with control ISH with a sense riboprobe (right). (**b**) $Nlgn1$ mRNA was expressed broadly (left; Cx, cortex; St, striatum). A high-magnification image (right) of the cortex (dotted box) revealed $Nlgn1$ mRNA in all cortical layers. (**c**) Double ISH detected $Gapdh$ (left) and $Nlgn1$ (middle) in individual layer 2/3 neurons (top). Representative images of neighboring neurons (arrowheads) showing differential $Nlgn1$ mRNA expression in spite of relatively consistent $Gapdh$ mRNA levels (bottom). (**d**) Cumulative probability distribution of $Nlgn1:Gapdh$ ISH fluorescence ratios from ten sets (one per section, three mice) of ten randomly picked neighboring neurons (yellow circle in **c**).
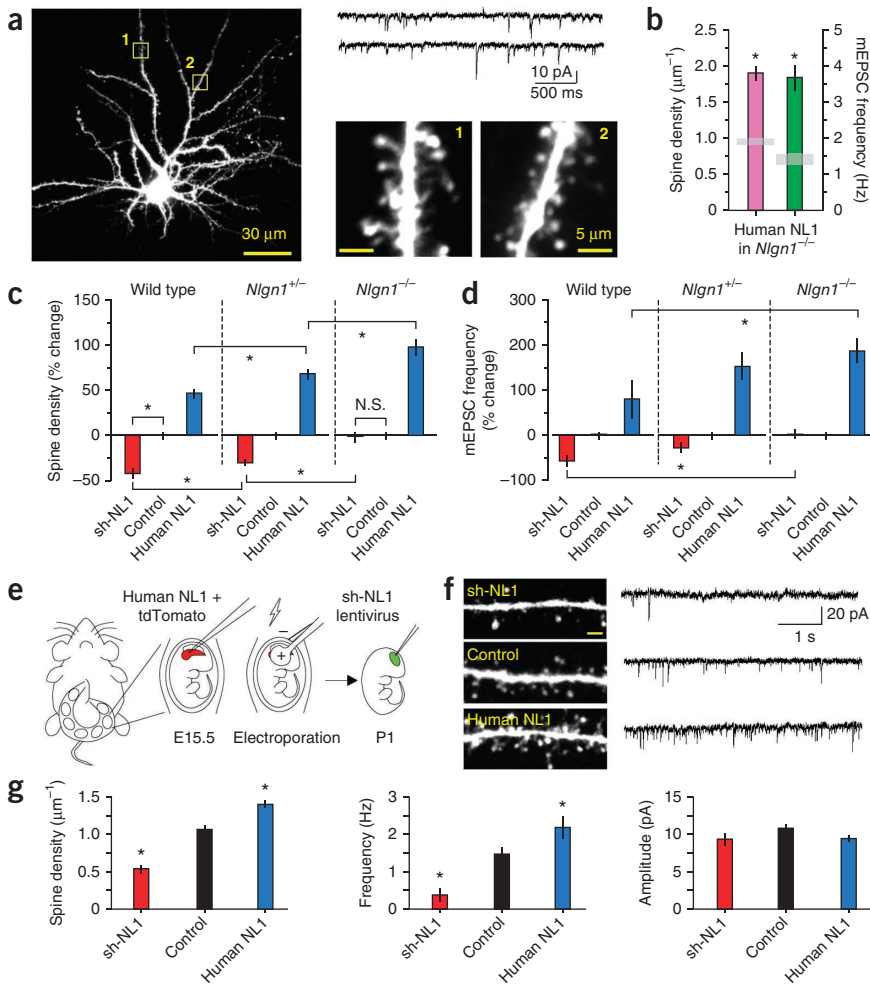
Figure 7 Relative levels of NL1 determine spine number *in vivo* via intercellular interactions. (**a**) Representative *NLGN1*-transfected neuron in an *Nlgn1*$^{-/-}$ mouse showing spines and mEPSCs. (**b**) Average spine density and mEPSC frequency from human NL1–expressing neurons in *Nlgn1*$^{-/-}$ mice. The gray boxes indicate the values mean ± s.e.m. in control neurons. (**c,d**) Spine density and mEPSC frequency were differently affected by manipulating NL1 levels up (human NL1) or down (sh-NL1) depending on the levels of NL1 in the surrounding neurons. (**e**) Schematic of the experimental design. Mice were *in utero* electroporated with human NL1 + tdTomato, followed by injection of sh-NL1–encoding lentivirus into cortex at P1. (**f**) Left, representative images of spines from layer 2/3 pyramidal neurons infected with sh-NL1 lentivirus (top), neighboring controls (middle) or electroporated with human NL1 + tdTomato (bottom). Right, representative mEPSCs for the same three neuronal classes. Scale bars represent 2 μm, 20 pA and 1 s. (**g**) Average spine density, mEPSC frequency and amplitude in sh-NL1, control and hNL1 neurons analyzed in the same slices. Error bars represent s.e.m. *$P < 0.05$ on *post hoc* multiple comparison tests relative to control. N.S., $P > 0.05$. Error bars represent s.e.m.

$P < 0.05$ versus wild type). In contrast, sh-NL1 #4, a second, very efficient shRNA, greatly reduced spine density (0.4 ± 0.04 spines per μm, 15 dendrites, $P < 0.05$ versus wild type).

Second, if the magnitude of transcellular gradients in NL1 levels determines the density of excitatory synapses, then spine density in a sparse subset of neurons that overexpress NL1

express NL1, indicating that transcellular interactions determine synapse number. These results were obtained without use of RNAi, demonstrating context-dependent defects in synapse numbers in neurons with constitutive genetic loss of NL1.

Gradients of NL1 levels exist and regulate spine number

To understand whether neuron-to-neuron variability in NL1 expression *in vivo* could support the competitive model presented above, we measured mRNA levels by fluorescence *in situ* hybridization (ISH) across cortical neurons (**Fig. 6**). *Nlgn1* mRNA was detected throughout all cortical layers without layer-specific expression (**Fig. 6a,b**). To determine the degree of variation of NL1 expression in cortical layer 2/3, we performed two-color fluorescence ISH of *Nlgn1* and *Gapdh* (**Fig. 6c**). Levels of endogenous *Nlgn1* mRNA expression largely varied from cell to cell compared with GAPDH (**Fig. 6c,d**), resulting in a larger coefficient of variation (GAPDH and NL1: *Gapdh*, $26.1 \pm 1.6\%$, $n = 10$ fields; *Nlgn1*, $37.7 \pm 4.3\%$, $n = 10$; $P < 0.05$).

To directly test *in vivo* whether transcellular gradients of NL1 expression level regulate synapse number, we examined a variety of conditions in which NL1 expression was higher or lower in a cell relative to its neighbors (**Fig. 7** and **Supplementary Fig. 5**). First, we examined whether spine density is regulated in a dose-dependent manner by NL1. We took advantage of a specific sh-NL1, sh-NL1 #9, which partially reduced NL1 levels (**Fig. 1a**). When transfected into neurons of wild-type animals, sh-NL1 #9 reduced spine density only slightly (0.7 ± 0.03 spines per μm, 27 dendrites,

in *Nlgn1*$^{-/-}$ mice should be higher than in neurons that overexpress NL1 in wild-type mice. Indeed, spine density in *NLGN1*-transfected neurons in *Nlgn1*$^{-/-}$ mice was very high (1.9 ± 0.1 spines per μm, 10 neurons, 17 dendrites; *NLGN1*-transfected neurons in *Nlgn1*$^{+/+}$ mice, 1.4 ± 0.1 spines per μm, 11 neurons, 22 dendrites; $P < 0.05$; **Fig. 7a,b**). Increased density of spines was accompanied by increased mEPSC frequency, indicating that more functional synapses had been made (*NLGN1* in *Nlgn1*$^{-/-}$, 3.67 ± 0.35 Hz, $n = 8$; *NLGN1* in *Nlgn1*$^{+/+}$, 2.19 ± 0.43 Hz, $n = 6$, $P < 0.05$; **Fig. 7a,b**).

Furthermore, across many manipulations, the magnitude of changes in spine density and mEPSC frequency induced by manipulations of NL1 depend on the NL1 content of neighboring neurons. The effects of NL1 knockdown were reduced in the *Nlgn1*$^{+/-}$ hemizygote mice and were completely absent in *Nlgn1*$^{-/-}$ mice (percent change in spine density: *Nlgn1*$^{+/+}$, $-42 \pm 6\%$; *Nlgn1*$^{+/-}$, $-30 \pm 3\%$; *Nlgn1*$^{-/-}$, $-1 \pm 5\%$ compared with the matched background; percent change in mEPSC frequency: *Nlgn1*$^{+/+}$, $-58 \pm 12\%$, $n = 8$; *Nlgn1*$^{+/-}$, $-27 \pm 12\%$, $n = 8$; *Nlgn1*$^{-/-}$, $1 \pm 11\%$, $n = 9$; **Fig. 7c,d**). Conversely, the effects of overexpression of NL1 were more notable when NL1 levels were reduced in neighboring cells (percent change in spine density: human NL1 in *Nlgn1*$^{+/+}$, $47 \pm 5\%$; human NL1 in *Nlgn1*$^{+/-}$, $68 \pm 6\%$; human NL1 in *Nlgn1*$^{-/-}$, $102 \pm 9\%$ compared with the matched background; percent change in mEPSC frequency: human NL1 in *Nlgn1*$^{+/+}$, $79 \pm 43\%$, $n = 6$; human NL1 in *Nlgn1*$^{+/-}$, $155 \pm 30\%$, $n = 10$; human NL1 in *Nlgn1*$^{-/-}$, $187 \pm 28\%$, $n = 8$; **Fig. 7c,d**). The changes in spine density and synapse number seen with perturbation of NL1 levels were

not a result of variability in these parameters across animals, as they were observed when wild-type, sh-NL1–expressing and human NL1–overexpressing neurons in the same slice were compared (spine density: sh-NL1, 0.53 ± 0.06 spines per μm, $n = 12$ neurons, 22 dendrites; wild type, 1.06 ± 0.05 spines per μm, $n = 9$ neurons, 15 dendrites; human NL1, 1.40 ± 0.05 spines per μm, $n = 8$ neurons, 19 dendrites; mEPSC frequency: sh-NL1, 0.37 ± 0.17 Hz, $n = 5$; wild type, 1.47 ± 0.18 Hz, $n = 7$; human NL1, 2.18 ± 0.30 Hz, $n = 5$ neurons; mEPSC amplitude: sh-NL1, 9.3 ± 0.8 pA; wild type, 10.8 ± 0.5 pA; human NL1, 9.4 ± 0.4 pA; **Fig. 7e–g**). Thus, spine density and mEPSC frequency in each cell are determined not by the cell's absolute level of NL1, but by the difference in its expression of NL1 relative to neighboring neurons.

DISCUSSION

The function of NL1 *in vivo* in the regulation of synaptogenesis and the number of excitatory synapses per neuron has been controversial, with some studies concluding direct functions of NL1 in both processes and other studies proposing a later function of NL1 in activity-dependent synapse validation[19,27,42]. To resolve some of these controversies, we examined, in a variety of genetic contexts, synaptic and cellular properties of cortical layer 2/3 pyramidal neurons whose levels of NL1 had been altered. Furthermore, we compared the effects of sparse and global manipulations to determine whether synapses are sensitive to the absolute levels of NL1 in an individual cell or to relative differences in NL1 in comparison with neighboring neurons.

We found that the defects in cellular development depended on the context in which NL1 was perturbed. Loss of NL1 in all cells, and in only a subset of cortical layer 2/3 neurons, equally altered the level of extra-synaptic and synaptic NMDARs, consistent with previous results[19,24–26]. However, when NL1 levels were decreased or increased in one cell relative to its neighbors, additional functions of NL1 in the regulation of activity-dependent spinogenesis and synapse number were revealed. Thus, neurons that had relatively high levels of NL1 grew new spines more readily, leading to increased spine density and functional synapse number. In contrast, neurons with relatively low levels of NL1 were deficient in the same parameters.

Transcellular gradients in NL1

Neuroligins have been proposed to act in the initial stages of synapse formation to promote synaptogenesis[27]. This hypothesis was supported by the observation that the number of synapses and spine density decreased with reduction of neuroligin and increased with enhanced expression[19,28–34]. Recently, it was alternatively proposed that neuroligins function in synapse specification and validation such that synapses initially form in a neuroligin-independent manner but their stabilization or maintenance require validation by neuroligins[19]. However, each hypothesis has been tested in different systems and supported differentially by *in vitro* and *in vivo* data. Furthermore, often the effects of NL1 on synapse number were seen following RNAi-mediated knockdown, which is susceptible to difficult-to-exclude off-target effects[43].

To directly examine the role of NL1 *in vivo* in synapse formation, we manipulated NL1 expression levels in either a subset of neurons or in all neurons and examined the effects on *de novo* activity-dependent spinogenesis and mature synapse number. All of our analyses were performed in cortical layer 2/3 pyramidal neurons. We conclude that relative differences in NL1 across neurons determine the potential for initial synapse formation, which likely underlies the changes in excitatory synapse density observed in more mature neurons. Notably, we found that the effects of RNAi against NL1 are specifically the results of NL1 loss, as they were prevented by coexpression of human

NL1, recapitulated by several shRNA sequences and, most notably, not seen when the shRNA was expressed in $Nlgn1^{-/-}$ mice. This last control should be considered the gold standard for off-target effects in RNAi-based studies.

Thus, *in vivo* analyses indicate that NL1 levels in a cell that are high relative to its neighbors put the cell at advantage in the process of synapse formation, resulting in higher density of excitatory synapses. These results were confirmed *in vitro*, as cultured GFP-labeled $Nlgn1^{-/-}$ layer 2/3 pyramidal neurons only displayed defects in spine density when mixed with $Nlgn1^{+/+}$ neurons. The intercellular or intersynapse processes that determine spine number and growth may include competition for binding to presynaptic neurexins and displacement by NL1 of other neurexin-binding partners, such as leucine-rich repeat transmembrane neuronal proteins[44,45].

Regulation of individual synapses by NL1

We also found that the absolute and relative levels of NL1 regulate individual synapses. Loss of NL1 in all contexts decreased NMDAR-evoked currents and calcium influx by ~50%, and spine morphology was altered by sparse manipulation of NL1, consistent with previous reports[19,29]. These morphological changes are likely to have a functional effect, as spines with large heads and long necks trap signaling molecules for longer periods[46,47]. Indeed, we found altered Ca^{2+} signaling in spines and dendrites of neurons with altered NL1 expression. This may also affect the temporal and spatial profiles of signaling pathways involved in synaptic formation, maturation and plasticity. For example, protein kinase A is anchored in the dendrite at rest, but the activated catalytic subunit moves into the spine and facilitates induction of long-term potentiation[48], a process that may be hampered by narrow and long spine necks.

Our findings resolve previous conflicts in the literature by demonstrating that the effects of NL1 on synaptogenesis and synapse number are highly context dependent. The combination of our *in vitro* and *in vivo* results suggest that defects in synaptogenesis and synapse number are revealed in NL1-lacking neurons if neighboring neurons express NL1. Similarly, the degree of perturbation of synapse number is graded depending on the relative differences in NL1 across neurons. Our findings resolve previous conflicts in the literature by demonstrating that the effects of NL1 on synaptogenesis and synapse number are highly context dependent.

METHODS

Methods and any associated references are available in the online version of the paper.

Note: Supplementary information is available in the online version of the paper.

ARTICLES

1. Katz, L.C. & Shatz, C.J. Synaptic activity and the construction of cortical circuits. *Science* **274**, 1133–1138 (1996).
2. Sanes, J.R. & Yamagata, M. Many paths to synaptic specificity. *Annu. Rev. Cell Dev. Biol.* **25**, 161–195 (2009).
3. Huberman, A.D., Feller, M.B. & Chapman, B. Mechanisms underlying development of visual maps and receptive fields. *Annu. Rev. Neurosci.* **31**, 479–509 (2008).
4. Moody, W.J. & Bosma, M.M. Ion channel development, spontaneous activity, and activity-dependent development in nerve and muscle cells. *Physiol. Rev.* **85**, 883–941 (2005).
5. Grutzendler, J., Kasthuri, N. & Gan, W.B. Long-term dendritic spine stability in the adult cortex. *Nature* **420**, 812–816 (2002).
6. Hofer, S.B., Mrsic-Flogel, T.D., Bonhoeffer, T. & Hubener, M. Experience leaves a lasting structural trace in cortical circuits. *Nature* **457**, 313–317 (2009).
7. Trachtenberg, J.T. *et al.* Long-term *in vivo* imaging of experience-dependent synaptic plasticity in adult cortex. *Nature* **420**, 788–794 (2002).
8. Alvarez, V.A. & Sabatini, B.L. Anatomical and physiological plasticity of dendritic spines. *Annu. Rev. Neurosci.* **30**, 79–97 (2007).
9. Dalva, M.B., McClelland, A.C. & Kayser, M.S. Cell adhesion molecules: signaling functions at the synapse. *Nat. Rev. Neurosci.* **8**, 206–220 (2007).
10. Scheiffele, P. Cell-cell signaling during synapse formation in the CNS. *Annu. Rev. Neurosci.* **26**, 485–508 (2003).
11. Südhof, T.C. Neuroligins and neurexins link synaptic function to cognitive disease. *Nature* **455**, 903–911 (2008).
12. Contractor, A. *et al.* Trans-synaptic Eph receptor-ephrin signaling in hippocampal mossy fiber LTP. *Science* **296**, 1864–1869 (2002).
13. Yamagata, M., Sanes, J.R. & Weiner, J.A. Synaptic adhesion molecules. *Curr. Opin. Cell Biol.* **15**, 621–632 (2003).
14. Song, J.Y., Ichtchenko, K., Sudhof, T.C. & Brose, N. Neuroligin 1 is a postsynaptic cell-adhesion molecule of excitatory synapses. *Proc. Natl. Acad. Sci. USA* **96**, 1100–1105 (1999).
15. Varoqueaux, F. *et al.* Neuroligins determine synapse maturation and function. *Neuron* **51**, 741–754 (2006).
16. Ichtchenko, K. *et al.* Neuroligin 1: a splice site–specific ligand for beta-neurexins. *Cell* **81**, 435–443 (1995).
17. Ichtchenko, K., Nguyen, T. & Sudhof, T.C. Structures, alternative splicing, and neurexin binding of multiple neuroligins. *J. Biol. Chem.* **271**, 2676–2682 (1996).
18. Jamain, S. *et al.* Reduced social interaction and ultrasonic communication in a mouse model of monogenic heritable autism. *Proc. Natl. Acad. Sci. USA* **105**, 1710–1715 (2008).
19. Chubykin, A.A. *et al.* Activity-dependent validation of excitatory versus inhibitory synapses by neuroligin-1 versus neuroligin-2. *Neuron* **54**, 919–931 (2007).
20. Poulopoulos, A. *et al.* Neuroligin 2 drives postsynaptic assembly at perisomatic inhibitory synapses through gephyrin and collybistin. *Neuron* **63**, 628–642 (2009).
21. Durand, C.M. *et al.* Mutations in the gene encoding the synaptic scaffolding protein SHANK3 are associated with autism spectrum disorders. *Nat. Genet.* **39**, 25–27 (2007).
22. Feng, J. *et al.* High frequency of neurexin 1beta signal peptide structural variants in patients with autism. *Neurosci. Lett.* **409**, 10–13 (2006).
23. Jamain, S. *et al.* Mutations of the X-linked genes encoding neuroligins NLGN3 and NLGN4 are associated with autism. *Nat. Genet.* **34**, 27–29 (2003).
24. Blundell, J. *et al.* Neuroligin-1 deletion results in impaired spatial memory and increased repetitive behavior. *J. Neurosci.* **30**, 2115–2129 (2010).
25. Kim, J. *et al.* Neuroligin-1 is required for normal expression of LTP and associative fear memory in the amygdala of adult animals. *Proc. Natl. Acad. Sci. USA* **105**, 9087–9092 (2008).
26. Soler-Llavina, G.J., Fuccillo, M.V., Ko, J., Sudhof, T.C. & Malenka, R.C. The neurexin ligands, neuroligins and leucine-rich repeat transmembrane proteins, perform convergent and divergent synaptic functions *in vivo*. *Proc. Natl. Acad. Sci. USA* **108**, 16502–16509 (2011).
27. Scheiffele, P., Fan, J., Choih, J., Fetter, R. & Serafini, T. Neuroligin expressed in non-neuronal cells triggers presynaptic development in contacting axons. *Cell* **101**, 657–669 (2000).
28. Boucard, A.A., Chubykin, A.A., Comoletti, D., Taylor, P. & Sudhof, T.C. A splice code for trans-synaptic cell adhesion mediated by binding of neuroligin 1 to alpha- and beta-neurexins. *Neuron* **48**, 229–236 (2005).
29. Chih, B., Engelman, H. & Scheiffele, P. Control of excitatory and inhibitory synapse formation by neuroligins. *Science* **307**, 1324–1328 (2005).
30. Dean, C. *et al.* Neurexin mediates the assembly of presynaptic terminals. *Nat. Neurosci.* **6**, 708–716 (2003).
31. Graf, E.R., Zhang, X., Jin, S.X., Linhoff, M.W. & Craig, A.M. Neurexins induce differentiation of GABA and glutamate postsynaptic specializations via neuroligins. *Cell* **119**, 1013–1026 (2004).
32. Levinson, J.N. & El-Husseini, A. Building excitatory and inhibitory synapses: balancing neuroligin partnerships. *Neuron* **48**, 171–174 (2005).
33. Nam, C.I. & Chen, L. Postsynaptic assembly induced by neurexin-neuroligin interaction and neurotransmitter. *Proc. Natl. Acad. Sci. USA* **102**, 6137–6142 (2005).
34. Prange, O., Wong, T.P., Gerrow, K., Wang, Y.T. & El-Husseini, A. A balance between excitatory and inhibitory synapses is controlled by PSD-95 and neuroligin. *Proc. Natl. Acad. Sci. USA* **101**, 13915–13920 (2004).
35. Kwon, H.B. & Sabatini, B.L. Glutamate induces *de novo* growth of functional spines in developing cortex. *Nature* **474**, 100–104 (2011).
36. Bloodgood, B.L. & Sabatini, B.L. Nonlinear regulation of unitary synaptic signals by CaV(2.3) voltage-sensitive calcium channels located in dendritic spines. *Neuron* **53**, 249–260 (2007).
37. Sabatini, B.L., Oertner, T.G. & Svoboda, K. The life cycle of Ca^{2+} ions in dendritic spines. *Neuron* **33**, 439–452 (2002).
38. Barrow, S.L. *et al.* Neuroligin1: a cell adhesion molecule that recruits PSD-95 and NMDA receptors by distinct mechanisms during synaptogenesis. *Neural Dev.* **4**, 17 (2009).
39. Jung, S.Y. *et al.* Input-specific synaptic plasticity in the amygdala is regulated by neuroligin-1 via postsynaptic NMDA receptors. *Proc. Natl. Acad. Sci. USA* **107**, 4710–4715 (2010).
40. Buffelli, M. *et al.* Genetic evidence that relative synaptic efficacy biases the outcome of synaptic competition. *Nature* **424**, 430–434 (2003).
41. McClelland, A.C., Hruska, M., Coenen, A.J., Henkemeyer, M. & Dalva, M.B. Trans-synaptic EphB2–ephrin-B3 interaction regulates excitatory synapse density by inhibition of postsynaptic MAPK signaling. *Proc. Natl. Acad. Sci. USA* **107**, 8830–8835 (2010).
42. Chubykin, A.A. *et al.* Dissection of synapse induction by neuroligins: effect of a neuroligin mutation associated with autism. *J. Biol. Chem.* **280**, 22365–22374 (2005).
43. Alvarez, V.A., Ridenour, D.A. & Sabatini, B.L. Retraction of synapses and dendritic spines induced by off-target effects of RNA interference. *J. Neurosci.* **26**, 7820–7825 (2006).
44. de Wit, J. *et al.* LRRTM2 interacts with Neurexin1 and regulates excitatory synapse formation. *Neuron* **64**, 799–806 (2009).
45. Ko, J., Fuccillo, M.V., Malenka, R.C. & Sudhof, T.C. LRRTM2 functions as a neurexin ligand in promoting excitatory synapse formation. *Neuron* **64**, 791–798 (2009).
46. Santamaria, F., Wils, S., De Schutter, E. & Augustine, G.J. Anomalous diffusion in Purkinje cell dendrites caused by spines. *Neuron* **52**, 635–648 (2006).
47. Svoboda, K., Tank, D.W. & Denk, W. Direct measurement of coupling between dendritic spines and shafts. *Science* **272**, 716–719 (1996).
48. Zhong, H. *et al.* Subcellular dynamics of type II PKA in neurons. *Neuron* **62**, 363–374 (2009).

ONLINE METHODS

Plasmids. Mouse NL1 tagged with GFP on its C-terminal end[49] was a gift of N. Brose (Max Planck Institute). Human NL1 cDNA was purchased from OriGene (cat # SC127261). Four different target sequences for shRNA directed against mouse *Nlgn1* (sh-NL1 #1~4) were designed using the online utilities of the Whitehead Institute for Biomedical Research. 19–21-bp coding, loop and reverse complementary sequence nucleotides were synthesized (Integrated DNA Technologies) and ligated into pGUR, a vector that produces shRNA under an U6 promoter and EGFP under a CMV promoter[50]. Four additional sh-NL1 constructs (sh-NL1 #6~9) from Sigma were tested (cat # NM_138666). Western blot analysis showed that sh-NL1 #4 (5′-GGGGGAAGGGTTGAAGTTTGTTTCAA GAGAACAAACTTCAACCCTTCCCCCCTTTTTG-3′ and 5′-AATTCAAAA AGGGGGGAAGGGTTGAAGTTTGTTCTCTTGAAACAAACTTCAACCCT TCCCCC-3′) and #7 (5′-GGGCAGACCTTCACTCGAACTTTCTCGAGAAA GTTCGAGTGAAGGTCTGCCCCTTTTTG-3′ and 5′-AATTCAAAAAGGGG CAGACCTTCACTCGAACTTTCTCGAGAAAGTTCGAGTGAAGGTCTGC CC-3′) efficiently reduced NL1 levels.

Cell culture, transfection and viral infection. For the experiments to validate the efficiency of sh-NL1, 10^5 HEK293 cells were plated and 1 μg of NL1-GFP and 4 μg of sh-NL1 DNA was transfected using a calcium phosphate transfection kit (cat # 44-0052, Invitrogen). Cells were harvested 2 d later and the lysate was used for the western blotting.

Organotypic hippocampal slice cultures were prepared from 7–8-d-old Sprague Dawley rats[51]. The brain was taken out and immediately placed in chilled dissection media. Transverse hippocampal slices were chopped at 400–500-μm thickness and 4–6 slices were placed in a sterile culture plate insert (Millicell-CM, Millipore) in 6-well plates containing prewarmed media. DNA was biolistically transfected with a Helios Gene Gun (Biorad) 2 d after culturing. Bullets were made with 60 μg of DNA or, for the rescue experiments, 40 μg each of sh-NL1 and *NLGN1*. For the viral infection experiments, dissociated hippocampal cultures were prepared from 1-d-old rats. We plated 10^5 neurons in poly-D-lysine–coated 24-well plates. We added three infectious units of viruses per cell to the culture media 2 d later and harvested cells at 7–8 d after infection. Lentiviruses expressing sh-NL1 and control virus were purchased from Sigma (MISSION Lentiviral Transduction Particles; for sh-NL1 #7, cat #TRCN0000032021; for control, cat #SHC001V). For western blots, we used antibodies to NL1 (1:1,000, cat #129111), NL2 (1:1,000, cat #129202) and NL3 (1:1,000, cat #129311) (Synaptic Systems), and GAPDH (1:2,000, cat #2118 Cell Signaling Technology).

***In utero* electroporation.** All procedures for animal surgery and maintenance were performed following protocols approved by the Harvard Standing Committee on Animal Care and in accordance with US National Institutes of Health guidelines. To target neocortical layer 2/3 pyramidal neurons, we deeply anesthetized embryonic day 15.5 timed-pregnant female C57BL/6 mice (Charles River) by intraperitoneal injection of 2.5% Avertin (2, 2, 2-Tribromoethanol, vol/vol) or 2% isoflurane. Uterine horns were carefully exposed and 1-2 μl of DNA (1 μg μl^{-1}) were injected into one lateral ventricle. To visualize the injection, 0.005% fast green (vol/vol) was mixed with the DNA. Glass micropipettes for the injection were pulled, the tips broken to be ~50 μm in diameter, and beveled at 18° (Narishige). After injection, the embryo head was held with a tweezer with round plate electrodes (0.5-mm diameter) and electric pulses were delivered five times per second (50 V, 50 ms; CUY21 electroporator, NEPA GENE). Warm phosphate-buffered saline was dropped onto embryos periodically to prevent drying. The uterus was placed back into the pregnant mouse, and the anterior muscle and the skin were sutured separately. Pups were housed with the dam until they were needed. For the experiments shown in **Figure 7e–g**, pups *in utero* electroporated with human NL1 and tdTomato were intracranially injected on postnatal day 1 with 250 nl of ~10^9 titer lentivirus encoding sh-NL1 and GFP (Sigma MISSION Lentiviral Transduction Particles, TRCN0000032021-CMV-tGFP), using a protocol analogous to that described previously for adeno-associated viruses[52].

ISH and image analysis. Double fluorescence ISH was performed using a tyramide signal amplification method according to the manufacturer's instructions (NEL753001KT, PerkinElmer). Briefly, brains of 1-month-old mice were dissected and immediately frozen in liquid nitrogen. The brains were cut into 25 μm sections with a cryostat (Leica), postfixed in 4% paraformaldehyde (wt/vol), acetylated in 1% triethanolamine (vol/vol) and 0.25% acetic anhydride (vol/vol), prehybridized, and hybridized at 65 °C using the following anti-sense probes: *Nlgn1* (RP_050607_01_G08, Allen Institute for Brain Science), *Gapdh* (RP_050531_01_D11, Allen Institute for Brain Science), and *EGFP* (U55761, nt159-754). For *in vitro* transcription, *Nlgn1* cDNA was synthesized from Genscript and *Gapdh* cDNA was cloned out from a mouse cDNA library. Two fluorescein- or digoxigenin-labeled riboprobes generated by an *in vitro* transcription method (Promega) were hybridized simultaneously and stained by fluorescein or Cy3 chromogens, respectively. After staining, sections were mounted with Prolong Gold antifade reagent (P36934, Invitrogen). Images were collected by fluorescence microscopy using a Nikon Eclipse 80i microscope equipped with a Nikon DS-2 digital camera. For mRNA expression analysis, images were collected by confocal laser-scanning microscopy using a Zeiss LSM 510 META and processed using ImageJ (US National Institutes of Health). Images from wild-type brain sections were taken at 40× magnification and ten cells clustered in the layer 2/3 area were randomly selected per image for analysis. To quantify the *Nlgn1* and *Gapdh* mRNA expression level, areas with positive *in situ* signal for each gene in the same cell were measured using ImageJ and the coefficient of variation for *Nlgn1* and *Gapdh* mRNA levels were calculated from each image. The quantitative data from ten images were compiled and analyzed as cumulative probability distributions.

Spine analysis. Spine head area and length were analyzed using a MATLAB (MathWorks) program described previously[53]. For each spine, one line was drawn along the length of the spine (major axis) and the other line was drawn to cross the first line at the middle of the spine head where the fluorescent intensity is maximum (minor axis). Head area was calculated by counting the number of pixels inside the area where fluorescence intensity remained 30% of the maximal value. Spine length was designated as the distance to the point along the major axis where fluorescence dropped to 30% of the peak.

Acute slice preparation. C57BL/6 mice (17–25 d old) were deeply anesthetized with isoflurane and decapitated. The brain was rapidly removed and placed in chilled choline-based cutting solution containing 25 mM NaHCO$_3$, 1.25 mM NaH$_2$PO$_4$, 2.5 mM KCl, 7 mM MgCl$_2$, 25 mM glucose, 1 mM CaCl2, 110 mM choline chloride, 11.6 mM ascorbic acid and 3.1 mM pyruvic acid. Coronal sections of the brain were cut at 300-μm thickness using a Leica VT1000S vibratome (Leica Instruments) in cold cutting solution. Slices were transferred to artificial cerebrospinal fluid (ACSF) containing 127 mM NaCl, 2.5 mM KCl, 25 mM NaHCO$_3$, 1.25 mM NaH$_2$PO$_4$, 2 mM CaCl$_2$, 1 mM MgCl$_2$ and 25 mM glucose. Both cutting and ACSF solution were saturated with 95% O$_2$ and 5% CO$_2$ (pH 7.4). The slices were incubated at 20–22 °C for at least 1 h before recording.

Electrophysiology. A slice was transferred to a recording chamber perfused with ACSF. All voltage-clamp recordings were performed at room temperature, and current-clamp recordings at 32 °C. For voltage-clamp recordings, the electrode was filled with an internal solution containing 120 mM CsMeSO$_3$, 8 mM NaCl, 15 mM CsCl$_2$, 10 mM TEA-Cl, 10 mM HEPES, 2 mM QX-314, 4 mM MgATP and 0.3 mM Na$_2$GTP (pH 7.3). The pipette resistance was 3–4 MΩ. For current-clamping recording, the patch electrode was filled with 120 mM KMeSO$_4$, 5 mM KCl, 5 mM HEPES, 4 mM MgATP, 0.3 mM Na$_2$GTP and 10 mM phosphocreatine (pH 7.3). Patch pipettes were pulled with a micropipette puller (P-97, Sutter Instrument). Whole-cell recordings were made from cortical layer 2/3 pyramidal neurons. For Ca^{2+} imaging experiments, at least 10 min were allowed to pass after breaking the cell membrane before searching for a spine for analysis. For mEPSC recordings, cells were clamped at −60 mV in the presence of 10 μM CPP and 10 μM bicuculline. To measure AMPAR and NMDAR uEPSCs, uEPSCs were measured first at −60 mV and then at +40 mV. Glutamate uncaging-evoked EPSCs were measured in the presence of 10 μM D-serine, 1 μM tetrodotoxin, 1 μM ω-conotoxin-MVIIC, 20 μM nimodipine and 3 μM mibefradil. All recordings were made with a MultiClamp 700A or Axopatch 200B amplifiers (Axon Instruments).

Two-photon microscope and uncaging. Uncaging of MNI-glutamate and Ca^{2+} imaging was achieved using a custom-built microscope combining two-photon laser-scanning microscopy and two-photon laser photoactivation as previously

described[54]. Two mode-locked Ti:Sapphire lasers (Chameleon, Coherent) were used for imaging and uncaging at wavelengths of 840 nm and 720 nm, respectively. Alexa-594 (20 µM) and Fluo-5F (300 µM) were loaded in the cell through the recording patch pipette. 5 mM MNI-glutamate was perfused in the recirculating bath and a 500-µs-duration laser pulse at 720 nm was delivered to the target spot to release glutamate. Ca^{2+} transients shown in **Figures 2–4** are plotted in units of $\Delta G/G_{sat}$, which was calculated by dividing $\Delta G/R$ by G_{sat}/R. G_{sat}/R was measured in a 1:1 mixture of 1 M $CaCl_2$ and internal solution, which saturates the Ca^{2+} indicator. At least five consecutive responses (AMPAR uEPSCs, NMDAR uEPSCs and Ca^{2+} transients) were averaged from each spine. To deliver a constant stimulus to each spine, laser power was set to bleach red fluorescence in each spine head by ~40%[36].

Animals. B6;129 *Nlgn1*^{+/−} (heterozygous) mice were kindly provided by N. Brose (Max Planck Institute). Genotyping was accomplished by PCR of genomic DNA from the mouse tail. For genotyping, we used primers 428 (5-GAGCGCGCG CGGCGGAGTTGTTGAC-3′), 430 (5′-GTGAGCTGAATCTTATGGTTAGA TGGG-3′) and 561 (5′-CGGTCAACAAACCTACTCAGAATCAGG-3′). Data shown in **Figures 1**, **3** and **7** were obtained from *Nlgn1*^{−/−} and littermate control *Nlgn1*^{+/+} resulting from heterozygous mating. Both male and female mice were used for the experiments.

Statistics. The Kolmogorov-Smirnov test was used to determine significance of differences in spine morphology. To determine significant differences of success rate of spinogenesis, we used the Fisher's exact test. For all other experiments, statistical significance was judged using a Student's *t* test (two-sided) or one-way ANOVA followed by Newman-Keuls multiple comparison *post hoc* tests. $P < 0.05$ was judged as significant.

49. Dresbach, T., Neeb, A., Meyer, G., Gundelfinger, E.D. & Brose, N. Synaptic targeting of neuroligin is independent of neurexin and SAP90/PSD95 binding. *Mol. Cell. Neurosci.* **27**, 227–235 (2004).
50. Tavazoie, S.F., Alvarez, V.A., Ridenour, D.A., Kwiatkowski, D.J. & Sabatini, B.L. Regulation of neuronal morphology and function by the tumor suppressors Tsc1 and Tsc2. *Nat. Neurosci.* **8**, 1727–1734 (2005).
51. Stoppini, L., Buchs, P.A. & Muller, D. A simple method for organotypic cultures of nervous tissue. *J. Neurosci. Methods* **37**, 173–182 (1991).
52. Kozorovitskiy, Y., Saunders, A., Johnson, C.A., Lowell, B.B. & Sabatini, B.L. Recurrent network activity drives striatal synaptogenesis. *Nature* **485**, 646–650 (2012).
53. Sturgill, J.F., Steiner, P., Czervionke, B.L. & Sabatini, B.L. Distinct domains within PSD-95 mediate synaptic incorporation, stabilization, and activity-dependent trafficking. *J. Neurosci.* **29**, 12845–12854 (2009).
54. Carter, A.G. & Sabatini, B.L. State-dependent calcium signaling in dendritic spines of striatal medium spiny neurons. *Neuron* **44**, 483–493 (2004).
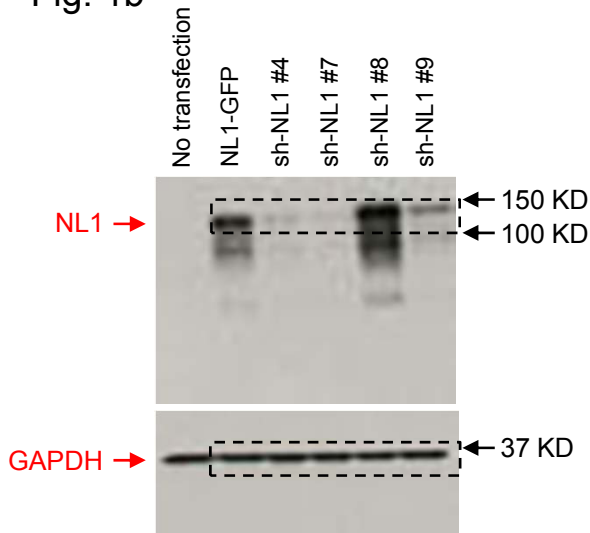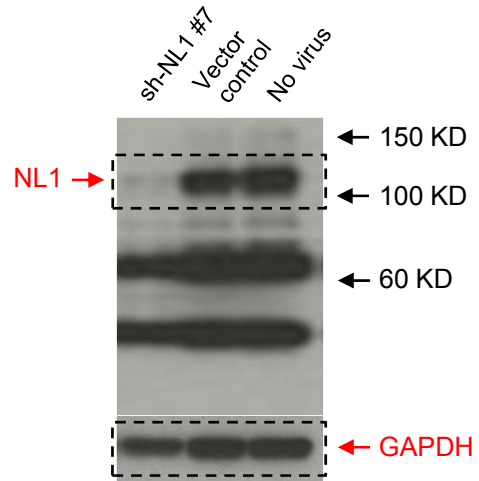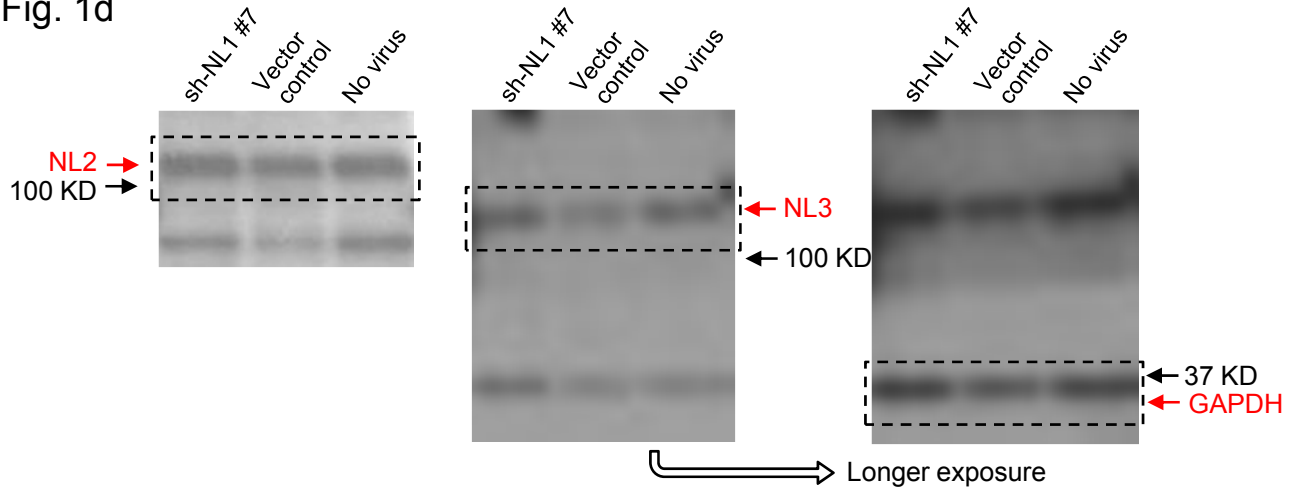
Fig. 1b

No transfection
NL1-GFP
sh-NL1 #4
sh-NL1 #7
sh-NL1 #8
sh-NL1 #9

NL1 → ← 150 KD
← 100 KD

GAPDH → ← 37 KD

Fig. 1c

sh-NL1 #7
Vector control
No virus

← 150 KD
NL1 → ← 100 KD
← 60 KD
← GAPDH

Fig. 1d

sh-NL1 #7
Vector control
No virus

NL2 →
100 KD →

sh-NL1 #7
Vector control
No virus

← NL3
← 100 KD

sh-NL1 #7
Vector control
No virus

← 37 KD
← GAPDH

Longer exposure

Supplementary Figure 1 Full images of western blots shown in the main figures

Bands within dashed line boxes are shown in Figure 1.
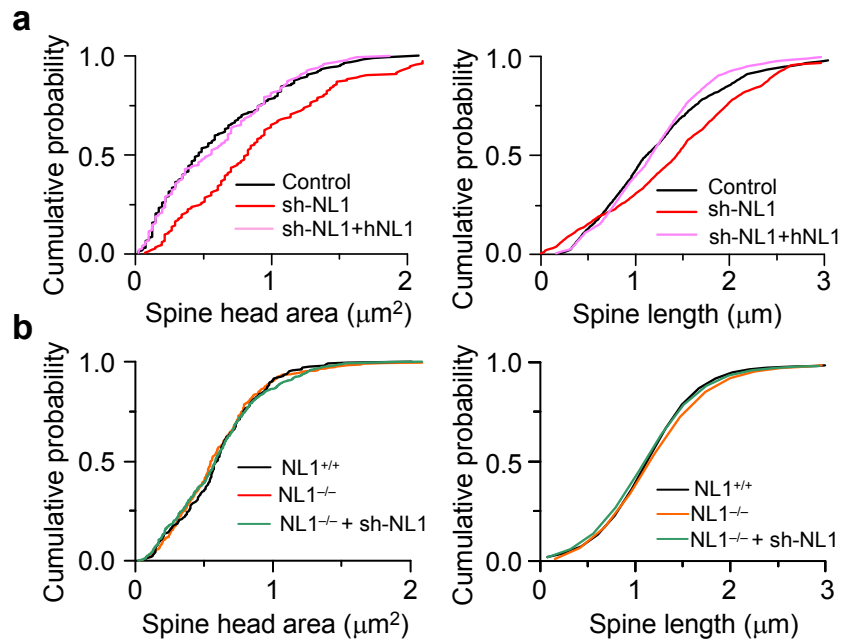
Supplementary Figure 2 Cumulative plots of spine head area and length

(a) Cumulative plots of spine head area and length from neurons transfected with the sh-NL1 #7 (sh-NL1), GFP (control), sh-NL1#7 and human NL1 (hNL1).

(b) Cumulative plots of spine head area and length from neurons of indicated genotypes.
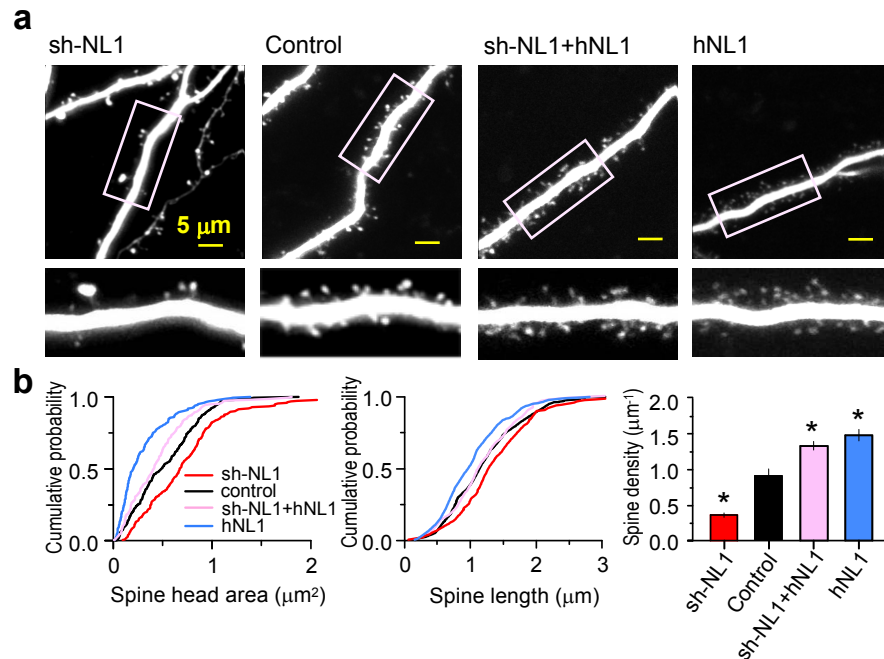
Supplementary Figure 3 Postsynaptic expression of NL1 regulates spine morphology and density in CA1 pyramidal neurons in organotypic hippocampal slices

(a) Representative images of dendritic spines of hippocampal CA1 pyramidal neurons transfected with the sh-NL1, GFP (control), sh-NL1#7 and hNL1, or hNL1 alone. The areas indicated by the white boxes are shown at higher magnification below.

(b) Cumulative distributions of apparent spine head areas (*left*), lengths (*middle*), and average spine density (*right*) measured from hippocampal CA1 neurons in organotypic slice cultures of the genotypes shown in panel (a). Error bars represent s.e.m.
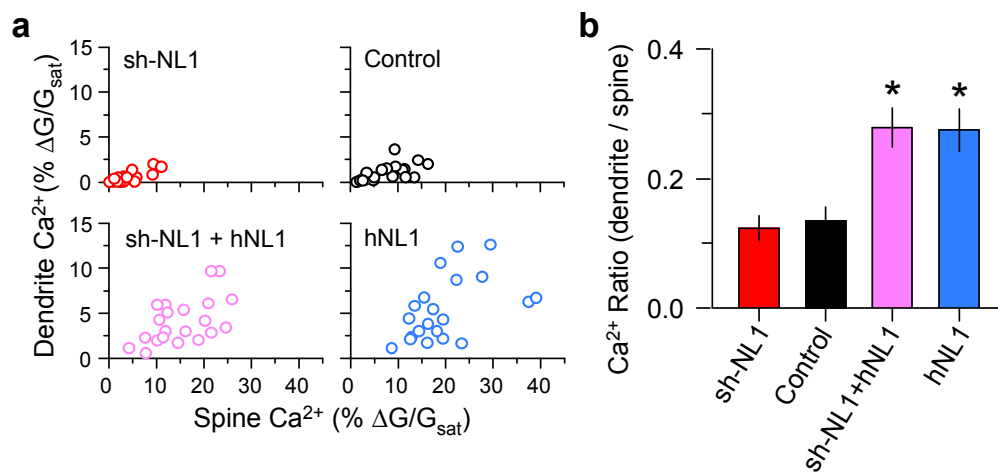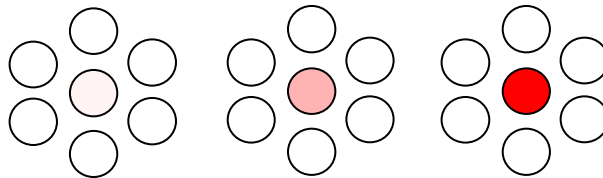
Supplementary Figure 4 Relative Ca^{2+} accumulation in the dendrite is increased by hNL1 overexpression

(a) Glutamate was photoreleased near the spine head and the Ca^{2+} transient peaks from the spine head and neighboring dendrite shaft were measured as described in Figure 2. Measurements from individual spines are plotted as open circles. Note that dendritic Ca^{2+} increased more steeply than spine Ca^{2+} when hNL1 was transfected (rescued and hNL1 groups).

(b) Average ratios of Ca^{2+} transient amplitudes in the dendrite relative to the spine, showing increased relative dendritic Ca^{2+} in rescued and hNL1 transfected neurons. Error bars represent s.e.m.

Absolute change
(cell-autonomous)

Relative change
(trans-cellular)
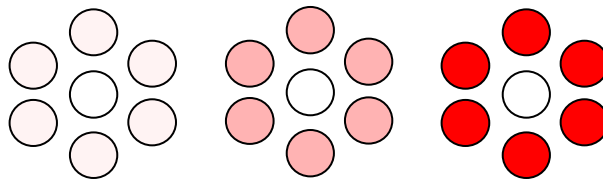
Supplementary Figure 5 Schematics of absolute and relative regulation of synapse number by NL1 expression

In the top, cell-autonomous model, changes in the level of expression of NL1 (red levels) in the center cell influence its own synapse number independent of the NL1 levels in the surrounding neurons. In the bottom, trans-cellular model, synapse number in the center cell is affected by the changes in NL1 levels of neighboring cells.